

Evolutionary Games, Complex Networks and Nonlinear Analysis for Epileptic Seizures Forecasting

Roberto Zingone, Chiara Mocenni, Dario Madeo

Department of Information Engineering and Mathematics, University of Siena,
Siena, Via Roma, 56, 53100, Italy

Abstract

Epileptic seizures detection and forecasting is nowadays widely recognized as a problem of great significance and social resonance, and still remains an *open, grand challenge*. Furthermore, the development of mobile warning systems and wearable, non invasive, advisory devices are increasingly and strongly requested, from the patient community and their families and also from institutional stakeholders. According to the many recent studies, exploiting machine learning capabilities upon intracranial EEG (iEEG), in this work we investigate a combination of novel game theory dynamical model on networks for brain electrical activity and nonlinear time series analysis based on recurrences quantification. These two methods are then melted together within a supervised learning scheme and finally, prediction performances are assessed using EEG scalp datasets, specifically recorded for this study. Our study achieved mean sensitivity of 70.9% and a mean time in warning of 20.3%, thus showing an increase of the improvement over chance metric from 42%, reported in the most recent study, to 50.5%. Moreover, the real time implementation of the proposed approach is currently under development on a prototype of a wearable device.

1 Introduction

Brain is universally recognized as one of the most complex systems in nature. Historically, complex systems have been extensively studied from physical and mathematical point of view [1] and many different kind of models have been proposed to describe the functioning of the brain.

As a complex system, it shows a huge number of interacting components (the number of neurons is estimated at roughly 100 billion) exhibiting hierarchical, spatially distributed and self-organizing structures, whose activity is driven by nonlinear mechanisms [2].

Although the fundamental biological elements (neurons) are well known, their particular physical network of connections, joined to their non-linear interactions, harden the analysis and modeling of the system itself. Moreover, it is well known that couple of brain areas, corresponding to *populations* of neurons, have correlated or anti-correlated dynamics.

After decades of research in the field of neurological diseases, such epilepsy [3, 4, 5], with alternating phases of optimism and pessimism [6, 7], very recent studies have paved the way for a cautious optimism about the possibility to predict epileptic seizures [8, 9].

These studies have been mainly focused on improving *artificial intelligence* approaches, and using large dataset of intracranial electroencephalography data (iEEG) [10, 11], substantially developing black-box models through the use of *invasive* measures of cerebral voltage, somehow in

competition with methods belonging to the field of dynamic systems [12, 13, 14, 15, 16]. At the same time, less attention has been paid to *mixed* approaches, combining dynamic models *and* machine learning techniques using *non-invasive* measures, such as scalp electroencephalography data (EEG).

Our intent is to exploit the high modularity of the brain, highlighting the role of connectivity [17] between areas using EEG signals, and the description of these interactions by using competitive models. Indeed, the electrical dynamics of brain suggests that areas may interact upon activation and inhibition mechanisms

Particularly suited to model the above mechanisms are *Graph Theory* [18] and *Evolutionary Game Theory* [19]: the former let us describe in a very natural way the network of connections where areas are the nodes of a graph, connected to each other through links, described by an *adjacency matrix*, while the latter provides us a mathematical model of the evolution of dynamical, competitive interactions. A powerful tool joining together Graph Theory and Evolutionary Game Theory is the Evolutionary Games on Networks (EGN) [20, 21, 22], allowing us to describe the dynamical behavior of game interactions between players (the areas) arranged on a network of connections. In this framework we consider areas as finite *populations* of neurons, interacting among themselves and choosing, at each time instant, one of two available strategies: *activation* and *inhibition*. Each area can have different behaviors with respect to the others, since it could exhibit imitation or opposition, in other words it chooses each move by imitating (or not) nearby connected areas.

In this work we apply the EGN equation to model EEG recordings of epileptic subjects. This approach, combined with well-known non linear methods based on Recurrence Quantification Analysis (RQA) [23, 24, 25, 26, 27], could unveil new insights about the epileptic phenomenon and lead, not only to the fulfilling of the primary need of seizure detection, but also to the more challenging goal of seizure forecasting.

The graphical abstract of all phases developed in the present work are reported in Figure 1.

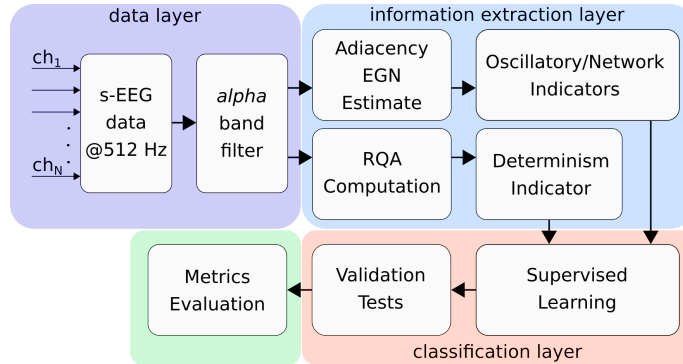


Figure 1: System logic view

2 Materials and Methods

2.1 Dataset

EEG is a *non-invasive* standard monitoring technique to record brain electrical activity, primarily acquired through electrodes on the scalp and has been widely adopted almost in every research field

involving normal or pathological brain activity [25, 28, 26, 29, 30].

Data acquisition has been done in clinical environment, at the Department of Medicine, Surgery and Neuroscience of the University of Siena in 2017, using standard international 10 – 20 system and consisted of 29 – 30 channels sampled at 512 Hz.

For the purpose of the present work we used a set of EEG recordings containing a total of 20 seizures belonging to different subjects under continuous clinical monitoring for the evaluation of epileptic focus resection. In this framework, several sequences of at least 5 consecutive seizures have been considered.

For each EEG signal, only the *alpha* band has been adopted. Indeed, frequencies in this band are sufficiently low in order to exclude artifacts such as for example ocular movements and eye blinks, arising at the delta band (< 4 Hz), typically at 1-2 Hz.

Furthermore, working with a *narrow* band has several advantages: i) it strongly weakens the effects of other artifacts such muscular or cardiac ones; ii) it allows to exclude *a priori* power grid artifacts; iii) it allows to reduce the preliminary *pre-processing* stage only to a *filtering* stage, avoiding the need of manual procedures (and therefore with the external support of an expert clinical neurologist). Moreover, it doesn't require the use of semi-automatic artifact removal methods, such as ICA (Independent Component Analysis) or PCA (Principal Component Analysis), complex and highly computationally expensive; iv) empirically, many epileptic seizures manifest themselves as oscillations with typical frequencies in the order of 6-10 peaks per second; v) higher frequency bands are normally associated with higher cognitive functions.

2.2 EGN model

Evolutionary game theory, is a powerful tool to study how particular agents change their behavior over time due to their reciprocal interactions. Recently it has been shown that evolutionary game theory on graphs is also suitable to describe the brain dynamics with respect to the one-to-one relations between cerebral areas [22]. Here it is assumed that the brain is composed by N entities, called areas, each grouping a huge number of elementary components (neurons). The activity of each area is monitored by means of standard acquisition techniques like EEG. High activity values means that a given area is activating, while lower values stands for inhibition. Each area is labeled by $v \in \{1, \dots, N\}$ and it is assumed to be a player able to take decision - to activate or to inhibits itself. The corresponding state variable $x_v(t)$ is a number between 0 and 1 that quantify the activity level of the area at a particular time ($x_v = 0$ denotes full inactivation, $x_v = 1$ denotes full activation of the area, while $x_v \in (0, 1)$ denotes intermediate levels of activation). Dynamically, each area compares its activity level with others and it changes its state accordingly, in order to maximize a certain payoff function. This changing is performed by imitative or oppositive behavior of each area with respect to the connected areas.

Formally, we represent the brain as a network of connections between different areas (vertex). This is achieved by means of a graph, hereafter described by the adjacency matrix $A = \{a_{v,w}\}$. The values $a_{v,w}$ correspond to the weight of connection between areas v and w . Notice that this graph is directed, i.e. $a_{v,w} \neq a_{w,v}$.

Each area plays games with neighboring areas using a payoff matrix, B_v , defined as follows:

$$B_v = \begin{bmatrix} \sigma_{v,1} & 0 \\ 0 & \sigma_{v,2} \end{bmatrix},$$

where $\sigma_{v,1}$ and $\sigma_{v,2}$ are the payoff obtained by area v when its strategy as well as the strategy of any opponent is the same.

When area v plays against area w , the payoff of activation for v is $\sigma_{v,1}x_w$, while the payoff for inactivation is $\sigma_{v,2}(1 - x_w)$. Dynamically, area v changes the activation level according to the difference between these payoffs:

$$\Delta p_{v,w} = \sigma_{v,1}x_w - \sigma_{v,2}(1 - x_w) = (\sigma_{v,1} + \sigma_{v,2})x_w - \sigma_{v,2}$$

. When $\Delta p_{v,w}$ is positive, the activation level is increased; instead, for a negative difference, the inhibition is preferred. On the basis of all the difference payoff $\Delta p_{v,w}$ observed in all the interaction of v with neighboring areas w , the replicator equation on graphs for two strategies [20] is described by the following set of ODE:

$$\dot{x}_v = x_v(1 - x_v) \sum_{w=1}^N a_{v,w} \Delta p_{v,w}. \quad (1)$$

Remarkably, the set $[0, 1]$ is invariant for the previous equation, that is $x_v(t) \in [0, 1]$ for all time t . Moreover, notice that the sign of the derivative of x_v depends on $\sum_{w=1}^N a_{v,w} \Delta p_{v,w}$; in particular, if $\sum_{w=1}^N a_{v,w} \Delta p_{v,w} > 0$, the x_v will increase. Indeed, in this case, the outcome of activation is bigger than the outcome of inactivation.

Starting from real data (EEG signals), we can use this model in order to estimate the network of connections. The estimation problem reads as follows:

$$\hat{A} = \arg \min_A \sum_{t=1}^T \sum_{v=1}^N \|x_v(t) - z_v(t)\|^2, \quad (2)$$

where $x(v)_t$ is the solution of equation 1, while $z_v(t)$ is the observed time series. Notice that the estimation \hat{A} of the minimization problem (2) is the solution of a standard least-square problem, since there is a linear dependence between state variables and the parameters.

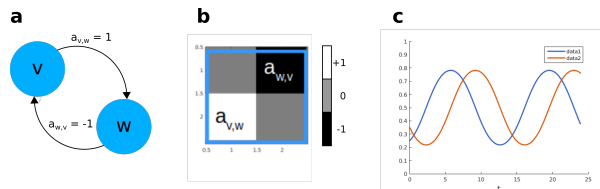


Figure 2: Basic oscillatory mechanism in 2-players game - **a**: graph representing the game, v mimics w and w reacts in opposition; **b**: corresponding adjacency matrix A , $a_{v,w} = 1$ and $a_{w,v} = -1$, diagonal is zero due to the lack of self-loops in the graph; **c**: corresponding time evolutions of the RE-G for a given initial condition.

The capabilities of equation (1) to model the brain dynamics can be understood by assuming $\sigma_{v,1} = \sigma_{v,2} = 1 \forall v$, and considering the simplest case with two players only ($N = 2$) [22]. When $a_{1,2} > 0$ and $a_{2,1} > 0$, then the two areas will imitate reciprocally, reaching at steady state a common intermediate level of cooperation. When $a_{1,2} < 0$ and $a_{2,1} < 0$, then the two areas will do the opposite of the other, and at steady state, one will be fully active, and the other will be fully inactive. Finally, when $a_{1,2} > 0$ and $a_{2,1} < 0$ (or $a_{1,2} < 0$ and $a_{2,1} > 0$), the mixture of imitative/opposite

mechanisms leads to the formation of oscillating behaviors (see Figure 2). Furthermore, adding a player, and thus playing a 3-players game, produces more types of oscillations (see Figure 3 to get a glimpse of how complexity in oscillatory behaviour evolves). As the number of areas increases,

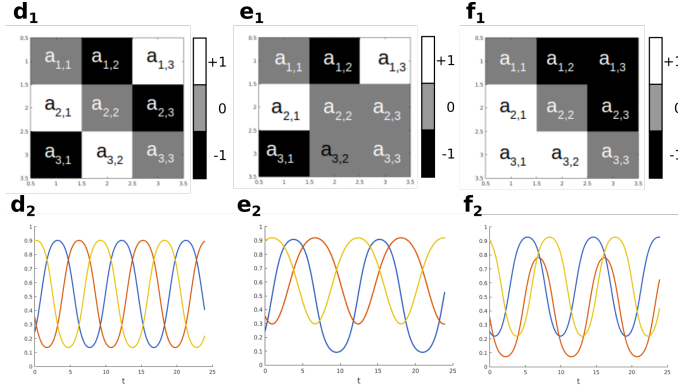


Figure 3: Adding oscillatory complexity, 3-players game examples - \mathbf{d}_1 , \mathbf{d}_2 : fully antisymmetrical adjacency matrix A ($a_{i,j} = -a_{j,i}$) and corresponding time evolutions of the system; \mathbf{e}_1 , \mathbf{e}_2 : adjacency matrix obtained from \mathbf{d}_1 disconnecting player 2 from player 3, ($a_{2,3} = 0$ and $a_{3,2} = 0$) and corresponding time evolutions of the system; \mathbf{f}_1 , \mathbf{f}_2 : fully antisymmetrical adjacency matrix A ($a_{i,j} = -a_{j,i}$) but with homogeneous sign distribution, and corresponding time evolutions of the system.

the formation of complex oscillatory patterns is fostered. Remarkably, the number of the recorded EEG channels for this study (or equivalently, the number of brain areas), ranges between $N = 29$ and $N = 31$.

These preliminary evidences indicate that the role of the network of connections is crucial to analyze, detect and predict changing behaviors of the brain activity due to pathologies like epilepsy. Fundamental indicators of the properties of the network are represented by the degree of each node DEG (i.e. the size of the neighborhood of each player), and the clustering coefficient, CC, (i.e. a measure that quantifies how the neighborhood of a node is close to be a clique) [31], both indicating the strength of a given node in the whole system. Besides these standard indicators, the number of anti-symmetrical couples of nodes (i.e. $\text{sign}(a_{v,w}) \neq \text{sign}(a_{w,v})$), hereafter named as AC, is related to the richness of the oscillating behavior of the system as shown in Figures 2 and 3, thus representing another important indicator for the considered system. The role of these indicator will be deeply analyzed in Section 3.2.1.

2.3 RQA

Recurrence Quantification Analysis (RQA) [23, 32, 33], is a nonlinear technique for analysis of time series, and it is grounded upon the concept of Recurrence Plot (RP). Given a trajectory in a phase space $x(t)$, the RP is formally defined as a matrix \mathbf{R} , which entries are the followings:

$$\mathbf{R}_{i,j} = \Theta(\epsilon - \|x_i - x_j\|), \quad (3)$$

where $x_i = x(i\Delta t)$, $x_j = x(j\Delta t)$, Δt is the sampling time, ϵ is a positive parameter, and Θ is the Heaviside step function. $\mathbf{R}_{i,j}$ is 1 when the trajectory x at time t_i is very close to itself at time t_j , and it represents a recurrence. Since any point is recurrent with itself, the RP always includes the diagonal line, for which $\mathbf{R}_{i,j} = 1, \forall i = j$, called Line of Identity (LOI). See Figure 4 for examples of RPs.

Notice that a real-world time series $s(t)$ (e.g. an EEG recording) represents an output of an underlying dynamical system. The phase space trajectory $x(t)$ of this dynamical system, used to build up the RP, can be reconstructed exploiting the Takens' embedding theorem [34]. In particular, at time t_i , the reconstructed trajectory is a point in a m -dimensional space, defined as

$$x_i = [s_i, s_{i+\tau}, \dots, s_{i+(m-1)\tau}],$$

where $s_i = s(i\Delta t)$, m is the embedding dimension (the minimum dimension such that there is no overlapping of the reconstructed trajectories), and τ is the delay time, representing a measure of correlation existing between two consecutive components of m -dimensional vectors used in the trajectory reconstruction.

The structures forming an RP (diagonal and vertical lines) encapsulate information on the dynamical system, and it has been shown that these can be used to detect dynamical transition such as chaos-order transitions [35] or chaos-chaos transitions [36]. In particular, the presence of diagonal structures means that the evolution of states is similar at different times and is often associated with deterministic/periodic processes, and the presence of vertical structures means that some states do not change or change slowly for some time, often associated with laminar states (in opposition from turbulent).

Quantitative information on these structures are obtained using the RQA, which provides a plethora of indicators to quantify the number and duration of recurrences of a dynamical system presented by its phase space trajectory. One of the most important is the so-called determinism [37]: it is the percentage of recurrence points forming diagonal lines longer than a minimal length l_{min} , and it is defined as follows:

$$DET = \frac{\sum_{l \geq l_{min}} lP(l)}{\sum_{l \geq 1} lP(l)} = \frac{\sum_{l \geq l_{min}} lP(l)}{\sum_{i,j} R(i,j)}, \quad (4)$$

where $P(l)$ is the number of diagonal lines of length l in the RP. Remarkably, the determinism is related with randomness/predictability of the underlying dynamical system: for instance, a random time series exhibits a sparse RP and hence a low value of determinism (close to 0); instead periodic time series show high values of determinism (close to 1), caused by a dense RP with many diagonal lines (see the subplot A of Figure 4).

In this work, we built RP matrices of the reconstructed phase space of each EEG recording for time windows of 10 seconds. In particular, we set embedding dimension $m = 3$ using the false nearest neighbors algorithm, and the delay time $\tau = 5$, determined as the first zero of the autocorrelation function [38, 39]; furthermore, the minimum length of diagonal lines (l_{min}) has been set equal to 20. Finally, a Theiler window of length 10 has been used to avoid the influence of temporally correlated points [25]. In Figure 4 we report an example of RP of a healthy subject (subplot B), and the RPs of an epileptic patient during the seizure few seconds after the onset (subplot C and D). For each time window, we evaluated the determinism which is thereafter used as a feature for the detection and forecasting phases. In order to meaningfully compare the determinism values over time, the parameter ϵ used for building the RPs has been chosen in order to guarantee that the percentage of recurrence points in each time window is almost constant.

2.4 Classification

In order to assess the predictive capacity of the proposed nonlinear methods, we relied upon a supervised machine learning technique, the support vector machine (SVM) [41], to create predictive models for forecasting future seizures.

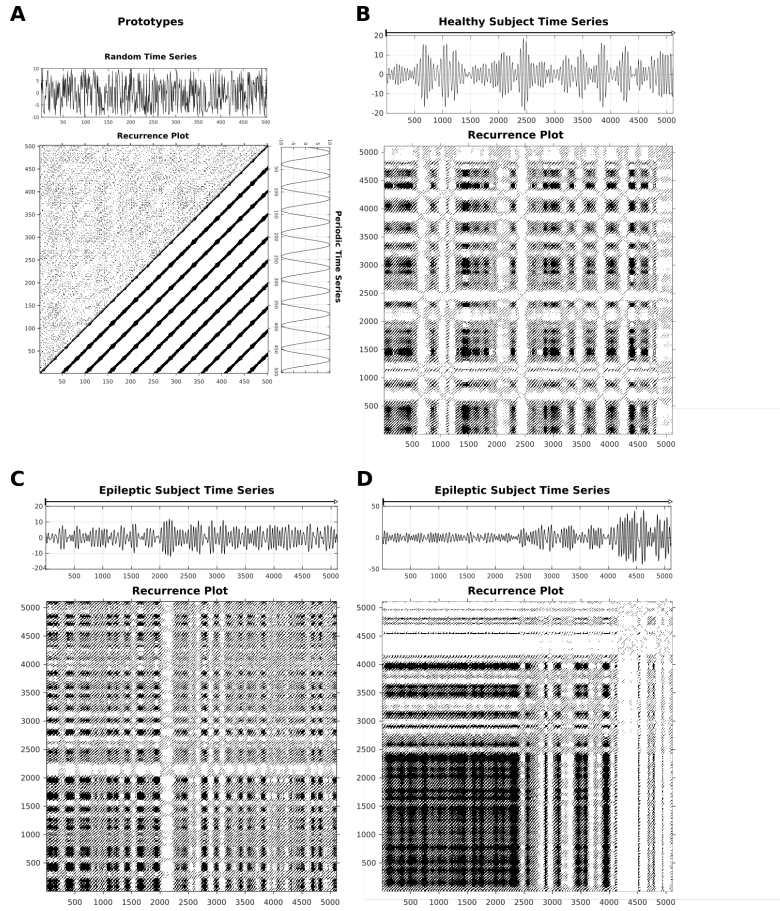


Figure 4: On the first row, subplot **A** shows the extremal prototypes of RPs achievable from *periodic* time series, whose lower-triangular portion of RP is composed by *diagonal* structures, and from *uniform, random* time series with the corresponding upper-triangular portion of RP showing a very low recurrence points percentage, with no structures and mainly consisting of *isolated* points. subplot **B** report an RP obtained from 10 seconds of a single channel from an healthy subject, which show a heterogeneous dynamic due to the non-uniformity of the structures. On the second row, subplot **C** shows 10 seconds of channel F8 time series, starting 17 seconds after the reported seizure onset (hence in the midst of the seizure, with regular, low amplitude oscillatons) and below the corresponding Recurrence Plot with very regular and homogenous patternn; subplot **D** shows another 10 second window of the same channel, starting 23 seconds after the reported onset and the corresponding Recurrence Plot showing sudden dynamical changes, highlighted by large white bands in the RP.

All the EGN and RQA features (DEG, CC, AC and DET) have been evaluated over time for each EEG channel. We will indicate with $DEG_v(t)$, $CC_v(t)$, $AC_v(t)$ and $DET_v(t)$, the degree, the clustering coefficient, the number of anti-symmetrical couples and the determinism at time t of the channel v . Moreover, also the average values of these features over the channels are used as additional features, namely $ADEG(t) = \langle DEG_v(t) \rangle$, $GCC(t) = \langle CC_v(t) \rangle$, $AAC(t) = \langle AC_v(t) \rangle$ and $ADET(t) = \langle DET_v(t) \rangle$, where $\langle \cdot \rangle$ denotes the average over the N channels. Using these $4(N + 1)$ features, we selected portion of data for the training (more details in Section 3.3). These have been conveniently labeled in a binary way as *pre-ictal* or *inter-ictal* and finally used to train the SVMs.

To avoid *overfitting* we performed a cross-validation, which is a powerful method to maximize the amount of data used for model training, and typically resulting in a model able to generalize better [42].

3 Results and Discussion

In the following subsections we illustrate: EGN model preliminary fitting properties and detection performance of the mean number of oscillating components global indicator on the first subject, detection performance of the mean determinism value global indicator plus local color-scaled determinism values indicators on the same patient and finally, classification and forecasting results on all the subjects.

3.1 EGN model fitting

In order to evaluate model performance we estimated the adjacency matrices A in consecutive non-overlapped windows of 0.5 seconds each, i.e. at 512 Hz each data window is composed of $256 \text{ samples} \times N$, the number of measured EEG channels.

Then we simulated back the system using starting samples of each window as initial conditions.

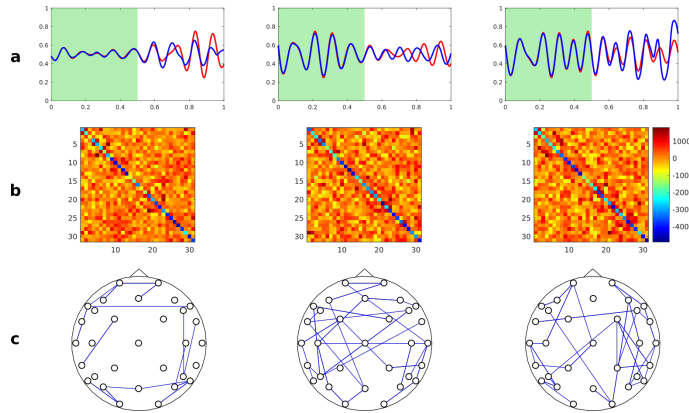


Figure 5: In first row **a** are reported three time series of F8 channel, picked at different times: 10 minutes, 5 minutes *before* the seizure onset and 10 seconds *after* the onset, respectively. The *red* signal is the *original* signal, the *blue* one is the *reconstructed* signal. The first 0.5 seconds are highlighted with a *green* background to indicate the amount of data used in the adjacency estimation. In second row **b** are reported the corresponding estimated adjacency matrices A . In the last row **c** are represented the underlying networks obtained after a proper thresholding.

Each simulation lasted for 1 second and as it can be seen from Figure 5, although for a single EEG channel over N channels, the EGN-*reconstructed* signal (the blue one) fits the *original* signal (the red one) with a very high precision, with a computed mean squared error (MSE) in the first 256 samples below 10^{-4} , then in the last 256 samples the reconstructed time series tend to lose *fidelity* from the original one and this could be evaluated in the increase of the corresponding MSE.

We used the previous MSE value as a reference to *certify*, in an empirical way, the ability of the model to accurately capture, or not, the dynamics of the underlying networked system.

The short time window obtained, in order to guarantee a high-quality EGN estimation, in the considered EEG context (low spatial resolution, high temporal resolution) could be explained considering that in [22] the *natural* frequencies arisen in the different fMRI context (high spatial resolution, low temporal resolution) were much lower, allowing to achieve longer simulation times, with comparable fitting performance.

3.2 Detection

The first question we wanted to address was if the EGN-based and RQA-based approaches were useful in discriminating between the phase of the epileptic discharge (with its physical manifestation) and the preceding (pre-ictal) phase, choosing a single indicator for both methods and looking in the seizure proximity of a subject.

3.2.1 EGN network-based feature

As remarked in Section 2.2, the role of the network is fundamental for assessing the dynamical properties of the considered model. Starting from the estimated adjacency matrices A , we can extract some indicators for the detection and the prediction of the epileptic seizures, namely the degree of each node $DEG_v(t)$, the clustering coefficient $CC_v(t)$ and the number of anti-symmetrical couples $AC_v(t)$, as well as their average values $ADEG(t)$, $GCC(t)$ and $AAC(t)$. All the $3(N + 1)$ indicators are suitably smoothed with a forward moving average window of 10 seconds. In this way, each point of the resulting time series *contains* informations from the 20 preceding adjacency estimations.

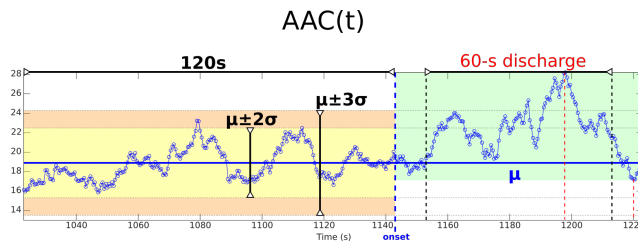


Figure 6: Subject no.1 - Average number of oscillating components on all channels ($AAC(t)$), in seizure 2 proximity. The average μ and standard deviation σ over over the considered time window of length 200 seconds are equal to 18.9 and 1.79, respectively.

In Figure 6 we report a fragment of $AAC(t)$ from the 2^{nd} seizure of subject no.1, considering 120s before the seizure onset, 10s as the time needed to the seizure to start manifesting itself with

its physical symptoms, 60s of seizure, and finally a further 10 seconds after the seizure, for a total time window 200 seconds. This time subdivision has been performed by an expert neurologist (epileptologist). The average μ and standard deviation σ over the time window of 200 seconds of $AAC(t)$ are also highlighted in Figure 6 (blue straight line for μ , yellow band for the interval $\mu \pm 2\sigma$, and orange band for the interval $\mu \pm 3\sigma$). $AAC(t)$ reaches the highest value approximately after 40 seconds after the onset with an excursion of more than 5 times the standard deviation. Remarkably, $AAC(t)$ remains above μ for the entire seizure duration. These aspects are also evident for the other 4 seizures of this subject, giving a first indication about the effectiveness of the number of anti-symmetrical couples as a discriminating feature.

3.2.2 RQA based feature

Determinism for each EEG channel was obtained from consecutive windows of 10 seconds with a 90% overlapping, thus resulting in a point for each second. The average determinism $ADET(t)$ has been computed on the same data fragment presented in the previous subsection and it has been reported in Figure 7. Here, y_2 and σ represent the average and the standard deviation of $ADET(t)$,

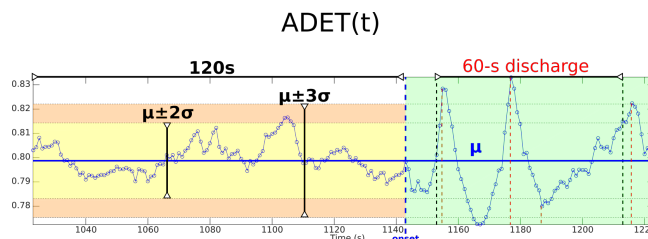


Figure 7: Subject no.1 - Average determinism on all channels, in seizure 2 proximity ($ADET(t)$). The average μ and standard deviation σ over the considered time window of length 200 seconds are equal to 0.8 and 0.01, respectively.

respectively, evaluated over the considered time windows. We observe that $ADET(t)$ lies almost everywhere in the range $\mu \pm 2\sigma$ before the onset. Instead, during the seizure we observe a strong oscillatory behavior. It is worthwhile to notice that these high amplitude oscillations reach peak values beyond the $\mu \pm 3\sigma$ band. This phenomenon is observed also in the other 4 seizures of the same subject.

Further analysis showed that this oscillatory behavior is the result of *local* determinism patterns. In Figure 8 we reported the single determinism values for each EEG channel ($DET_v(t)$). The color represents the determinism value of each channel over time, ranging from the smallest (blue) to the largest (red) value. The channels on the y-axis are ordered from the top with *left*-channels from $Fp1$ to $F9$, *central*-channels Fz, Cz, Pz and *right*-channels from $Fp2$ to $F10$.

A closer look shows that *left* channels reach smaller values (darker blue) and, in general *left* and *right* zones have inhomogeneous distribution of determinism. Specially, from Figure 8 we can appreciate the different distribution between *left* and *right* determinism values in the highlighted P1 and P2 zones preceding the onset, and from S1 to S6 zone after the onset: several local transition patterns are clearly visible immediately after the onset, from a basin of homogeneous lowest values $S3$ to the highest values (on average) zone $S4$, and from this zone (*all right* channels with greater values than left) to a zone composed by fewer *right* channels but with higher determinism values ($S6$), separated by an about 20-seconds wide homogeneous basin ($S5$) of low values.

The analysis of both the RQA-based *global* indicator and the *local* indicators gave us the second

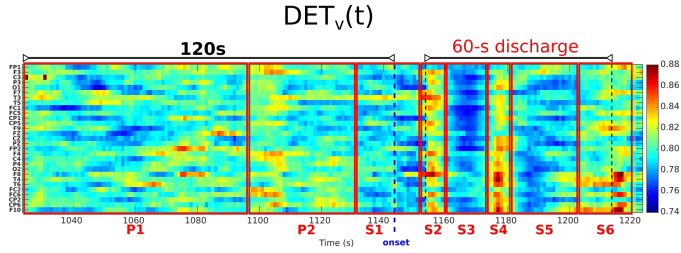


Figure 8: Subject no.1 - Color scaled determinism values of all channels, in seizure 2 proximity

indication about the effectiveness of this method in discriminating seizure patterns from non-seizure.

3.3 Validation

Previous analysis revealed several non-obvious global and local patterns in the seizure proximity, but at the same time cleared that, if the *manual* analysis of a few selected aggregated indicators such as $AAC(t)$, $ADET(t)$ and $DET_v(t)$ for short length recordings is a challenging task, the same manual approach to the full set of local and global indicators for long length recordings is unfeasible.

In order to tackle this complexity we adopted an *automatic*, supervised learning approach, substantially letting the system learn from sets of *labeled* training samples. This approach allowed to take into account the recognized and well established specificity of the epileptic phenomenon both in terms of specificity between patient and patient, and specificity between seizure and seizure of the same patient.

The full set of indicators described in Section 2.4 permits to generate an high-dimensional (equal to the total number of indicators) *features* space; a *generic* classifier has to decide if a point in this space belongs to the *inter-ictal* class or the *pre-ictal* class. We considered the latter as the representative class of possible events of interest that could culminate in a future seizure. Among the most used classifiers in the field literature, we selected SVM-type classifiers with a nonlinear, cubic kernel.

From the seizures' pool described in Section 2 we obtained 8 *feature* datasets of 5 seizures each. Each feature subset containing a single seizure lasted mainly from 20 minutes before the seizure onset plus 2 minutes after, for a total of 1200 samples per feature (1 feature sample per second), for the chosen $4(N + 1)$ features, only 3 recordings started in a shorter time interval, with the certified seizure onset after 12:45, 15:04 and 16:46 minutes, for a total duration of pre-seizure recordings equal to 390 minutes.

Datasets were then decomposed in training sets and validation sets: training sets have been created grouping feature data subsets from 4 seizures over the 5 available with a *leave-one-out* policy, generating all the possible permutations on the original 5-tuple of features and composing at the same time the *validation* sets with the features from the held-out seizure. In this way each feature dataset has 5 training sets with the corresponding validation sets.

We point out that among the possible permutations, only the one that leave the last seizure (in chronological order) for validation is considered as *prediction*, so at the end we have a total of 40 different training sets, of which 8 of them consist of seizures chronologically prior the seizure in the validation set.

Many studies adopt a single, *fixed* labelling policy in marking the *pre-ictal* class of interest, for example considering the features in the last 10 – 15 minutes before the onset. Instead we choosed a multiple, variable labelling policy for classification. In the following we will refer with P as the number of samples of each indicator composing the window for the *pre-ictal* class and with O as the time offset of the first *pre-ictal* sample of the window before the seizure onset. Five different

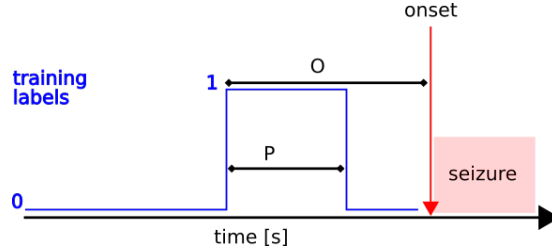


Figure 9: Classical labelling approach: ones are used for the pre-ictal class and zeroes for inter-ictal. Usually O is set equal to P, i.e. the pre-ictal examples are right before the onset.

windows were adopted, with P ranging from one minute to five minutes, i.e.:

$$P = \{60, 120, 180, 240, 300\} s,$$

(labeling in this way from a minimum of 4.55% to a maximum of 22.73% of indicators as pre-ictal), in combination with the offsets from a set of ten possible values, ranging from zero to ten minutes i.e.:

$$O = \{60, 120, 180, 240, 300, 360, 420, 480, 540, 600\} s.$$

Only the feasible combinations of these parameters, with $O \geq P$, were used in order to avoid overlapping of the samples with *in-seizure* data, for a total of 40 different types of classifier. Finally, each type has been trained on the 40 training sets previously described, with a k-fold cross-validation methodology in order to better optimize the amount of available data, leading to the generation of 1600 classifiers.

The mean training accuracy obtained from cross-validation was very high and above 99%, but this value could have been misleading, in the sense that trained classifiers could have learned very precisely the desired features from a relative low number of seizures samples and still not be able to generalize properly to new, unseen seizures. We assessed this problem measuring the classifiers performances with the held-out validation sets, never used from the cross-validation point of view.

To properly evaluate these performances we kept in mind that an hypothetical portable alarm system or device should raise an alarm on the basis of the classifier output, and this alarm could last in time [40]. Moreover the mapping between the output of the classifier and the resulting alarm could be not only 1 – 1 but in general $n - 1$, meaning that at least n consecutive *positive* outputs or *events* must be achieved by the classifier to let the device raise an alarm.

For this reason, as suggested in [10], we adopted the following metrics: the *sensitivity* (S), the true positive seizure prediction rate, i.e. if a seizure occurs while the system is in the alarm state then S is equal to 100%; the *time in warning* (TiW), the total duration of raised alarms (such red light indicators) in a monitored time window, i.e. if the system never raise an alarm its TiW is 0% and of course the corresponding S is 0% too, on the other side if the system raise alarms in a way that their total duration makes a TiW equal to 100%, surely it will achieve an S of 100% too. Both these cases (system always *off* or always *on*) are obviously useless in a real world scenario, but if

we consider these extremes as points in the plane with TiW on the x-axis and S on the y-axis, it remains a desirable *working* zone in the middle of these extremes, above the bisector line identified by the points that satisfy the equation $S = TiW$, or $IoC = 0$, where $IoC = S - TiW$ is defined as the improvement over chance [10].

In this framework, TiW and S strongly depend on the choice of the two aforementioned parameters: the first is the number of consecutive *events* labeled as *pre-ictal* by the classifier, that should be considered by the system or the device to raise an alarm, the second is the alarm duration. In the following we will refer to these parameters as E and W, respectively. For *each* classifier we performed a grid search varying E values between one and ten (events) and W from one second to five minutes with a one-second step, for a total of 3000 rounds per classifier computing S, TiW, IoC and prediction horizon (H) when $S = 100\%$ as the time interval between the alarm and the onset.

These metrics have been collected in 5 – D tensors with dimensions $d_1 \times d_2 \times d_3 \times d_4 \times d_5 = 40 \times 8 \times 5 \times 10 \times 300$, with d_1 the type of classifier, identified by P and O parameters; d_2 the number of datasets, d_3 the number of permutations on the dataset ($d_2 \times d_3 = 40$ is the number of *training sets*), d_4 and d_5 are E and W respectively. Each metric tensor contains 4800000 values.

In Figure 10 we report aggregated validation and prediction performances (the former are obtained on each possible permutations of the feature dataset, the latter only on the permutation that preserve the line of time) for each classifier, evaluating the mean sensitivity and the TiW box plots for all datasets and parameters combination in the five classifier groups identified by the P parameter, i.e. the size in seconds of the pre-ictal class.

In Table 1 we report the best validation performances with corresponding mean values obtained from each P_{i-th} group of classifiers, for all datasets, permutations and combinations of E and W parameters: summarizing the previous results and considering the corresponding mean IoC values,

P	S (%)	TiW (%)	IoC (%)	H (s)	O (s)
1	10.344	2.412	7.932	9.141	60
2	25.124	11.444	13.680	18.527	120
3	44.760	25.182	19.578	21.243	180
4	57.296	38.158	19.138	26.737	300
5	68.767	48.879	19.887	25.886	300

Table 1: Best validation performances on all datasets are reported for each P_{i-th} group of classifiers with mean sensitivity, mean time in warning, mean improvement over chance, mean prediction horizon and the time offset of the first pre-ictal sample with respect to the seizure onset.

P	S (%)	TiW (%)	IoC (%)	H (s)	O (s)
1	17.704	5.165	12.539	17.865	120
2	31.796	15.188	16.608	11.349	480
3	39.587	25.659	13.928	31.328	540
4	50.604	34.898	15.706	23.221	240
5	62.254	43.019	19.235	23.915	300

Table 2: Best prediction performances on all datasets are reported for each P_{i-th} group of classifiers with mean sensitivity, mean time in warning, mean improvement over chance, mean prediction horizon and the time offset of the first pre-ictal sample with respect to the seizure onset.

the best performance on *all datasets* from the validation point of view is achieved by the P_5 classifier

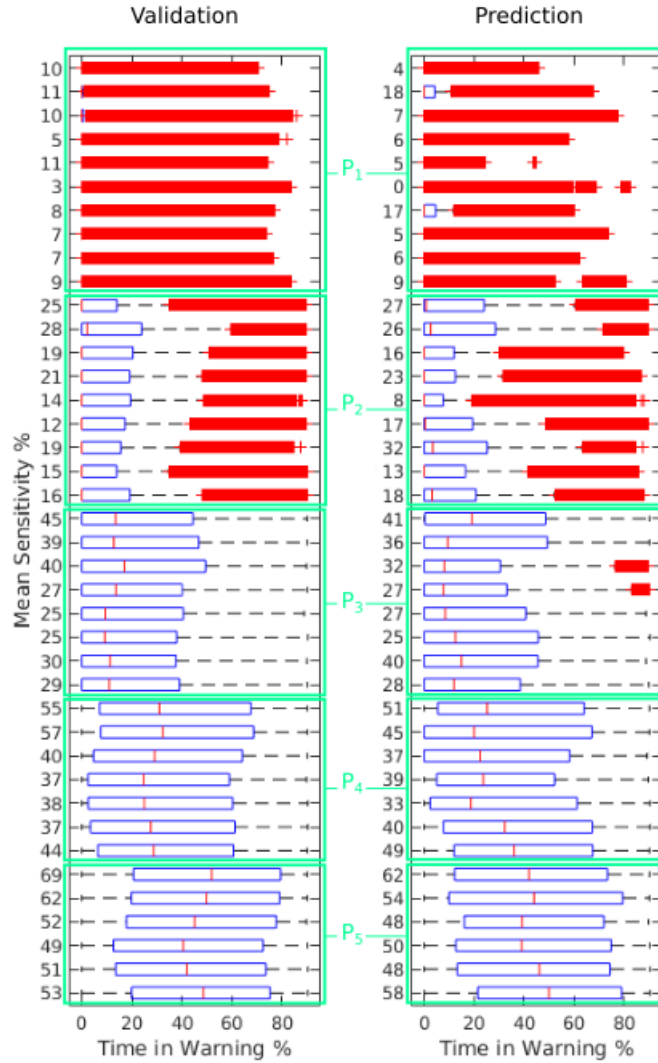


Figure 10: In both columns are reported for each classifier, the box plots of TiW values on all datasets, permutations, E and W parameters combinations: the central mark is the median TiW, the edges of the box are the 25th and 75th percentiles, and outliers are the red signed. Classifiers are grouped by P size with green boxes from P_1 to P_5 , i.e. from the smallest window considered (60s) at the top, to the largest window (300s) at the bottom, for each feasible, increasing O. On the left side of each box plot the corresponding mean(S) value (rounded) is reported. Left column reports the statistics considering validation performance on all the possible permutations of each dataset, so each box plot results from $1 \times d_2 \times d_3 \times d_4 \times d_5 = 120000$ data. Right column reports statistics considering *only* the performance on the chronologically ordered permutation, i.e. the one that leave in the validation set the features belonging to the last occurred seizure in time; each box plot in this column results from $1 \times d_2 \times 1 \times d_4 \times d_5 = 24000$ data.

with the 300 s window starting 300 seconds before the onset, which obtain an IoC equal to 19.89%, followed by P_3 classifier with the 180 second window starting 180 seconds before the onset and IoC equal to 19.58%, P_4 classifier with the 240 s window starting 300 seconds before the onset and an Ioc of 19.14%, P_2 classifier with 120 s window starting 120 s before the onset and IoC equal to 13.68% and finally P_1 classifier with 60 s window starting 60 s before the onset with an IoC of 7.93%.

In Table 2 we report the best prediction performances with corresponding mean values obtained

P	S (%)	TiW (%)	IoC (%)	H (s)	O (s)
1	29.712	9.785	19.927	33.056	120
2	58.871	30.212	28.659	51.646	120
3	77.745	55.043	22.702	42.342	180
4	87.437	70.471	16.966	46.148	240
5	96.513	77.791	18.722	44.259	360

Table 3: Best validation performances on all datasets, for reduced parameters sets E and W, are reported for each P_{i-th} group of classifiers with mean sensitivity, mean time in warning, mean improvement over chance, mean prediction horizon and the time offset of the first pre-ictal sample with respect to the seizure onset.

P	S (%)	TiW (%)	IoC (%)	H (s)	O (s)
1	49.983	13.036	36.948	51.197	120
2	66.076	35.605	30.471	28.223	480
3	86.159	60.571	25.587	77.524	540
4	98.526	71.163	27.364	52.437	240
5	93.543	74.381	19.162	50.892	360

Table 4: Best prediction performances on all datasets, for reduced parameters sets E and W, are reported for each P_{i-th} group of classifiers with mean sensitivity, mean time in warning, mean improvement over chance, mean prediction horizon and the time offset of the first pre-ictal sample with respect to the seizure onset.

from each P_{i-th} group of classifiers for all datasets, the permutation that preserve the last seizure as validation and combinations of E and W parameters: considering IoC values, the best result is still achieved from P_5 classifier with the same 300 s offset and an IoC of 19.23%, little lower than previous, followed by P_2 classifier (instead of the previous P_3 classifier) with a 480 s offset and IoC equal to 16.61%, a lower value compared to previous P_3 's IoC value but higher value than the corresponding previous P_2 value; then follow the P_4 classifier with a 240 s offset and a 15.70% IoC, lower than previous P_4 value, the P_3 classifier with 540 s offset and a Ioc value of 13.93%, lower than previous P_3 but higher than previous P_2 and at last P_1 with a 120 s offset and Ioc equal to 12.54%, higher than previous P_1 IoC.

Therefore the classifier trained with the last 300 s of pre-ictal samples before the onset reaches the best performance (*on average*, for all datasets and combinations of E and W parameters) in terms of sensitivity (68.76%-62.25%) and time in warning (48.87%-43.02%), in both validation and prediction performances.

We could benchmark this result with the results obtained in [10], corresponding to a mean sensitivity value of the prediction system equal to 69% over a mean time in warning of 27% noting that we achieve a comparable mean sensitivity, dropping at the same time about 16% – 22% on the mean time in warning performance. This drop is not surprising considering the different nature

of the datasets: our chosen features are builded upon clinical *non-invasive* s-EEG data, while data used in the benchmark study are *invasive* intracranial EEG data, with a huge difference in both data quality and reliability.

Moreover we could notice that we are not delimiting ranges for E and W parameters, the number

P	S (%)	TiW (%)	IoC (%)	H (s)	O (s)
1	46.325	17.106	29.219	39.640	300
2	66.291	40.142	26.149	49.986	480
3	83.336	64.754	18.582	56.921	480
4	93.435	78.637	14.799	32.892	300
5	99.669	83.529	16.140	34.491	360

Table 5: Best validation performances on all datasets, for the second reduced parameters sets E and W, are reported for each P_{i-th} group of classifiers with mean sensitivity, mean time in warning, mean improvement over chance, mean prediction horizon and the time offset of the first pre-ictal sample with respect to the seizure onset.

P	S (%)	TiW (%)	IoC (%)	H (s)	O (s)
1	70.902	20.380	50.522	69.990	120
2	61.921	33.068	28.852	32.965	300
3	100	71.005	28.995	43.375	240
4	100	78.231	21.769	32.500	240
5	99.793	82.964	16.829	41.554	360

Table 6: Best prediction performances on all datasets, for the second reduced parameters sets E and W, are reported for each P_{i-th} group of classifiers with mean sensitivity, mean time in warning, mean improvement over chance, mean prediction horizon and the time offset of the first pre-ictal sample with respect to the seizure onset.

of events needed by the system to raise the alarm and the duration of the alarm itself, respectively. If we continue to consider all dataset but restrict E in the set

$$E = \{1, \dots, 5\}$$

and W in the set

$$W = \{150, \dots, 300\} s$$

we obtain the following validation and prediction performances: from Table 3 we find that the best classifier now is, on average, the P_2 classifier with 120 offset with respect to the seizure onset, that scores a mean Ioc of 28.66% over a mean sensitivity of 58.88%, a mean time in warning of 30.2% and with a mean prediction horizon of 51.64 seconds. Comparison with results from Table 1 shows that improvement from the best previous 19.89% Ioc is mainly due to a substantial decreasing in TiW (from 48.88% to 30.2%) and at the same time a decreasing in S value (from 68.67% to 58.88%).

From the prediction point of view, Table 4 report that best classifier now is P_1 with a 120 s offset, reaching an average IoC value of 36.95% on mean sensitivity equal to 49.98% and mean time in warning equal to 13.03%, with a mean prediction horizon of 51.19 seconds. This mean Ioc value for a classifier is also closer to the 42% mean IoC value scored in [10].

Narrowing further set E in the range $\{1, 2\}$ lead to the following validation and prediction performances, summarized in Tables 5 and 6, respectively. The prediction results indicate that the

global performance of P_1 classifier with 120 s offset could be *refined*, achieving a mean IoC value of 50.52% resulting from a mean sensitivity of 70.9% and a mean TiW of 20.38% and a mean prediction horizon of about 70 seconds, improving the 42% IoC benchmark obtained in [10] of about 8%, resulting from an *increase* of 2% in the mean sensitivity and at the same time a *decrease* of more than 6% in the mean TiW.

Finally, the presented approach allow the possibility to evaluate these performances for each dataset *separately*, addressing in a pseudo-prospective manner the specificity between dataset and dataset. In the following we report in Table 7 validation performance on dataset 1, considering the previous sets for E and W: on all permutations the best classifier is P_1 with 300 s offset, which achieved a mean Ioc value of 41.92% over a mean sensitivity of 51.71% and time in warning of 9.78%, with a mean prediction horizon of 51.04 seconds.

Considering only the permutation that preserve the line of time, in Table 8 we see for dataset 1 that the best classifier remains P_1 but with a closer offset, with an *outstanding* mean Ioc of 92.16% over a 100% sensitivity and a 7.83% mean time in warning and with a prediction horizon of 102.6 s.

This mean also that, remarkably, a lot of valuable information about the incoming, *subject-specific* seizure is conveyed in the time interval going from 120 s to 60 s *before* the seizure onset, and this is exploited by the proposed features.

P	S (%)	TiW (%)	IoC (%)	H (s)	O (s)
1	51.709	9.788	41.921	51.041	300
2	59.152	26.096	33.056	45.678	180
3	88.874	50.565	38.309	47.807	180
4	93.430	69.548	23.882	50.666	600
5	100.000	81.016	18.984	39.520	300

Table 7: Best validation performances on dataset 1. For all permutations and reduced parameters sets E and W are reported for each classifier P-group, the mean sensitivity, mean time in warning, mean improvement over chance, mean prediction horizon and the time offset of the first pre-ictal sample with respect to the seizure onset.

P	S (%)	TiW (%)	IoC (%)	H (s)	O (s)
1	100	7.836	92.164	102.600	120
2	80	29.828	50.172	82.600	180
3	100	59.037	40.963	104.800	180
4	100	50.544	49.456	102.800	300
5	100	78.518	21.482	102.600	300

Table 8: Best prediction performances on dataset 1. For the last permutation and reduced parameters sets E and W are reported, for each classifier P-group, the mean sensitivity, mean time in warning, mean improvement over chance, mean prediction horizon and the time offset of the first pre-ictal sample with respect to the seizure onset.

This interesting result is reported in Table 9 for each dataset, showing that for these data it does not exists a unique, global classifier configuration, but instead several *specific* time intervals exist, not necessarily *long* ones and not necessarily *too close* to the onset, lasting just 60 or 120 seconds with valuable, predictive power, enabled by the *rich pool* of the proposed features, over the

D	S (%)	TiW (%)	IoC (%)	H (s)	P	O (s)
1	100	7.836	92.164	102.600	1	120
2	100	29.015	70.985	71.000	2	420
3	100	23.182	76.818	30.000	2	300
4	100	14.623	85.377	147.800	1	60
5	80	11.894	68.106	65.000	1	120
6	100	2.803	97.197	35.800	1	600
7	100	39.836	60.164	69.600	2	480
8	100	33.000	67.000	111.200	2	180

Table 9: Best prediction performances for each single dataset, with classifier parameters in previous E and W sets. S, TiW, IoC and H are mean values.

incoming next seizure.

4 Conclusions

In this work an hybrid approach based on a nonlinear dynamic model on network, namely the EGN, and a nonlinear time series method has been presented with application to the epileptic seizure detection and prediction from real *scalp* electroencephalogram data.

The proposed *mixed* approach permits to build, starting from noisy *real-world* data such as scalp EEG data, a classifier which obtain comparable performances with very recent studies in the field, notably based on *invasive* intracranial EEG data, in terms of mean sensitivity metric and better performances of the mean time in warning metric, scoring a mean improvement over chance of 50%, against a benchmark 42% value.

Furthermore, results obtained from *subject-specific* classification revealed novel insights about valuable information in specific short-lasting time intervals before seizure onset, information conveyed by the chosen features, thus reinforcing scalp based approaches, bearing in mind that s-EEG data represent the most obvious source for the development of new wearable warning devices.

However a major difficulty remains concerning the availability of statistically meaningful scalp EEG datasets in comparison with intracranial datasets, in terms of size (number of seizures), quality and reliability of data.

Addressing this point we are currently developing and building a prototype of a portable wearable device for seizure warning and continuous s-EEG recording, on which the proposed methods will be implemented to enhance the pool of available s-EEG seizures and the same toughen the features used.

Acknowledgments

DM, CM and RZ were partially supported by grant PANACEE (Prevision and analysis of brain activity in transitions: epilepsy and sleep) of Regione Toscana (Italy) - PAR FAS 2007-2013 1.1.a.1.1.2 - B22I14000770002.

Conflicts of interest

The authors declare no conflict of interest.

Appendix A - Examples on metrics evaluation

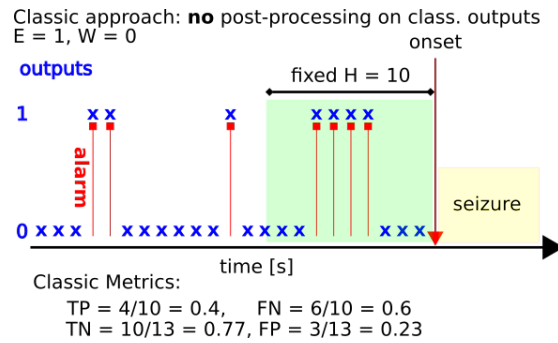


Figure 11: First example on metrics evaluation

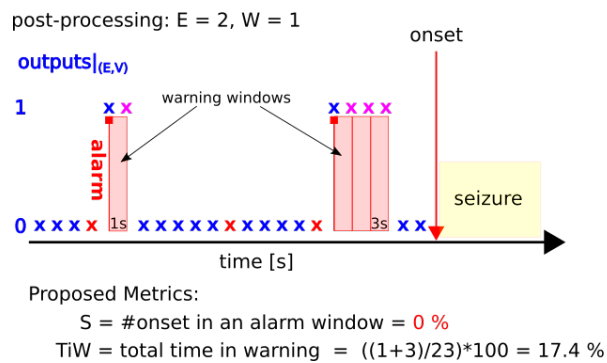


Figure 12: Second example on metrics evaluation

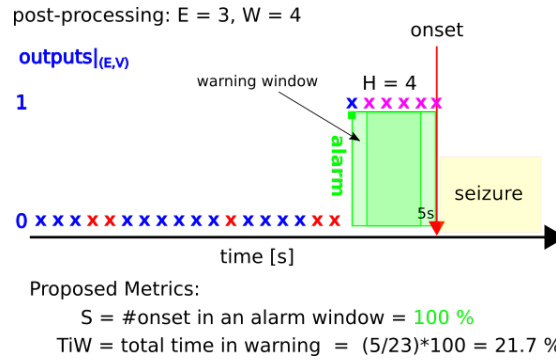


Figure 13: Third example on metrics evaluation

References

- [1] Strogatz, S. H. Nonlinear dynamics and chaos. Westview Press, 1994.
- [2] Madeo, D. Modeling and Identification of Networked and Distributed Complex Systems. Ph.D. Thesis, University of Siena, 2015.
- [3] Hocepiéd, G., Legros, B., Van Bogaert, P., Grenez, F., Nonclercq, A. Early detection of epileptic seizures based on parameter identification of neural mass model. *Comput. Biol. Med.* 2013, vol. 43, pp. 1773–1782.
- [4] Kramera, M. A., Kolaczykb, E. D., Kirschc, H. E. Emergent network topology at seizure onset in humans. *Epilepsy Research*, 2008, vol. 79, iss. 2–3, pp. 173–186.
- [5] Mormann, F., Kreuz, T., Rieke, C., Andrzejak, R. G., Kraskov, A., David, P., ... & Lehnertz, K. On the predictability of epileptic seizures. *Clinical neurophysiology*, 2005, 116(3), 569-587.
- [6] Lehnertz, K., Elger, C. E. Can Epileptic Seizures be Predicted? Evidence from Nonlinear Time Series Analysis of Brain Electrical Activity. *Phys. Rev. Lett.* 1998, vol. 80, pp. 5019–5022.
- [7] Mormann, F., Andrzejak, R. G., Elger, C. E., & Lehnertz, K. Seizure prediction: the long and winding road. *Brain*, 2006, 130(2), 314-333.
- [8] Stacey, W.C. Seizure Prediction Is Possible—Now Let’s Make It Practical. *EBioMedicine*, 2018.
- [9] Karoly, P. J., Ung, H., Grayden, D. B., Kuhlmann, L., Leyde, K., Cook, M. J., & Freestone, D. R. The circadian profile of epilepsy improves seizure forecasting. *Brain*, 2017, 140(8), 2169-2182.
- [10] Kiral-Kornek, I., Roy, S., Nurse, E., Mashford, B., Karoly, P., Carroll, T., ... & Grayden, D. Epileptic seizure prediction using big data and deep learning: toward a mobile system. *EBioMedicine*, 2017.
- [11] Cook, M. J., O’Brien, T. J., Berkovic, S. F., Murphy, M., Morokoff, A., Fabinyi, G., ... & Hosking, S. Prediction of seizure likelihood with a long-term, implanted seizure advisory system in patients with drug-resistant epilepsy: a first-in-man study. *The Lancet Neurology*, 2013, 12(6), 563-571.
- [12] Nguyen, N. A. T., Yang, H. J., & Kim, S. HOKF: High Order Kalman Filter for Epilepsy Forecasting Modeling. *Biosystems*, 2017, 158, 57-67.

- [13] Wendling, F., Benquet, P., Bartolomei, F., & Jirsa, V. Computational models of epileptiform activity. *Journal of neuroscience methods*, 2016, 260, 233-251.
- [14] Aarabi, A., He, B. Seizure prediction in hippocampal and neocortical epilepsy using a model-based approach. *Clinical Neurophysiology*, 2014, 125(5), 930-940.
- [15] Da Silva, F. L., Blanes, W., Kalitzin, S. N., Parra, J., Suffczynski, P., & Velis, D. N. Epilepsies as dynamical diseases of brain systems: basic models of the transition between normal and epileptic activity. *Epilepsia*, 2003, 44(s12), 72-83.
- [16] da Silva, F. H. L., Blanes, W., Kalitzin, S. N., Parra, J., Suffczynski, P., & Velis, D. N. Dynamical diseases of brain systems: different routes to epileptic seizures. *IEEE Transactions on Biomedical Engineering*, 2003, 50(5), 540-548.
- [17] Van Mierlo, P., Papadopoulou, M., Carrette, M. E., Boon, P., Vandenberghe, S., Vonck, K., Marinazzo, D. Functional brain connectivity from EEG in epilepsy: Seizure prediction and epileptogenic focus localization. *Progress in Neurobiology*, 2014, vol. 121, pp. 19-35.
- [18] Newman, M. E. J. *Networks, an Introduction*. Oxford University Press, 2010.
- [19] Hofbauer, J., Sigmund, K. *Evolutionary games and population dynamics*. Cambridge University Press, 1998.
- [20] Madeo, D., Mocenni, C. Game Interactions and dynamics on networked populations. *IEEE Trans. on Autom. Control*, 2015, vol. 60, is. 7, pp. 1801-1810.
- [21] Iacobelli, G., Madeo, D., & Mocenni, C. Lumping evolutionary game dynamics on networks. *Journal of Theoretical Biology*. 2016, 407, pp. 328-338.
- [22] Madeo, D., Talarico, A., Pascual-Leone, A., Mocenni, C., & Santarnecchi, E. An Evolutionary Game Theory Model of Spontaneous Brain Functioning. *Scientific Reports*. 2017, 7(1), 15978.
- [23] Marwan, N., Romano, M. C., Thiel, M., & Kurths, J. Recurrence plots for the analysis of complex systems. *Physics reports*, 2007, 438(5-6), 237-329.
- [24] Schinkel, S., Marwan, N., & Kurths, J. Brain signal analysis based on recurrences. *Journal of Physiology-Paris*, 2009, 103(6), 315-323.
- [25] Madeo, D., Castellani, E., Santarcangelo, E. L., Mocenni, C. Hypnotic assessment based on the Recurrence Quantification Analysis of EEG recorded in the ordinary state of consciousness. *Brain and Cognition*, 2013, vol. 83, is. 2, pp. 227-233.
- [26] Becker, K., Schneider, G., Eder, M., Ranft, A., Kochs, E. F., Zieglgänsberger, W., & Dodt, H. U. Anaesthesia monitoring by recurrence quantification analysis of EEG data. *PloS one*. 2010, 5(1), e8876.
- [27] Thomasson, N., Hoepfner, T. J., Webber Jr, C. L., & Zbilut, J. P. Recurrence quantification in epileptic EEGs. *Physics Letters A*, 2001, 279(1-2), 94-101.
- [28] Chiarucci, R., Madeo, D., Loffredo, M. I., Castellani, E., Santarcangelo, E. L., & Mocenni, C. Cross-evidence for hypnotic susceptibility through nonlinear measures on EEGs of non-hypnotized subjects. *Scientific reports*, 2014. 4, 5610.
- [29] Baghdadi, G., Nasrabadi, A. M. Effect of Hypnosis and Hypnotisability on Temporal Correlations of EEG Signals in Different Frequency Bands. *European Journal of Clinical Hypnosis*, 2009, 9(1).

- [30] Franaszczuk, P. J., Blinowska, K. J. Linear Model of Brain Electrical Activity - EEG as a Superposition of Damped Oscillatory Modes. *Biol. Cybern.* 1985, vol. 53, pp. 19-25.
- [31] Opsahl, T., Panzarasa, P. Clustering in weighted networks. *Social networks*, 2009, 31(2), 155-163.
- [32] Zbilut, J. P., & Webber Jr, C. L. Embeddings and delays as derived from quantification of recurrence plots. *Physics letters A*, 1992, 171(3-4), 199-203.
- [33] Webber Jr, C. L., & Zbilut, J. P. Dynamical assessment of physiological systems and states using recurrence plot strategies. *Journal of applied physiology*, 1994, 76(2), 965-973.
- [34] Takens, F. Detecting strange attractors in turbulence, in "Dynamical systems and turbulence". *Lect. Notes Math.* 1981, 898 366 - 381.
- [35] Trulla, L. L., Giuliani, A., Zbilut, J. P., & Webber Jr, C. L. Recurrence quantification analysis of the logistic equation with transients. *Physics Letters A*, 1996, 223(4), 255-260.
- [36] Marwan, N., Wessel, N., Meyerfeldt, U., Schirdewan, A., & Kurths, J. Recurrence-plot-based measures of complexity and their application to heart-rate-variability data. *Physical review E*, 2002, 66(2), 026702.
- [37] Mocenni, C., Facchini, A., & Vicino, A. Identifying the dynamics of complex spatio-temporal systems by spatial recurrence properties. *Proceedings of the National Academy of Sciences*, 2010, 107(18), 8097-8102.
- [38] Kantz, H., Schreiber, T. *Nonlinear time series analysis (Vol. 7)*. Cambridge university press. 2004.
- [39] Bradley, E., Kantz, H. Nonlinear time-series analysis revisited. *Chaos: An Interdisciplinary Journal of Nonlinear Science*, 2015, 25(9), 097610.
- [40] Snyder, D. E., Echauz, J., Grimes, D. B., & Litt, B. The statistics of a practical seizure warning system. *Journal of neural engineering*, 2008, 5(4), 392.
- [41] Russell, S. J., Norvig, P., Canny, J. F., Malik, J. M., & Edwards, D. D. *Artificial intelligence: a modern approach 2003*, (Vol. 2, No. 9). Upper Saddle River: Prentice hall.
- [42] Hastie, T., Tibshirani, R. & Friedman, J. *The Elements of Statistical Learning*. 2001. New York: Springer.